EPJ Web of Conferences **151**, 01004 (2017) DOI: 10.1051/epjconf/201715101004
LAM-16

Structural Analysis of Molten $NaNO_3$ by Molecular Dynamics Simulation

Shuta Tahara[1,*], *Hiroshi* Toyama[1], *Hironori* Shimakura[2], and *Takanori* Fukami[1]

[1]Department of Physics and Earth Sciences, Faculty of Science, University of the Ryukyus, Okinawa 903-0213, Japan

[2]Niigata University of Pharmacy and Applied Life Sciences, Niigata 956-8603, Japan

Abstract. MD simulation for molten $NaNO_3$ has been performed by using the Born-Mayer-Huggins-type potentials. The new structural features of molten $NaNO_3$ are investigated by several analytical methods. The coordination-number and bond-angle distributions are similar to those of simple molten salts such as NaCl except for the variation caused by the different size of the anion and cation. Na^+ ions are attracted toward O^- ions, and get separated from N^+ ions by Coulomb interactions. The distribution of the dihedral angle between NO_3^- plannar ionic molecules has also been investigated.

1 Introduction

$NaNO_3$ consists of Na^+ ions and NO_3^- ionic molecules, where three O^- ions in a NO_3^- molecule form an equilateral triangle around the central N^+ ion with a covalent bond between N^+ and O^- ions. $NaNO_3$ is a well-known component of explosives. Recently, the molten state of $NaNO_3$ has also been used for fabricating heat-storage materials for application in solar power generation [1-5]. Adya et al. for the first time investigated the microscopic atomic configuration and diffusion in molten $NaNO_3$ by means of X-ray diffraction measurement and molecular dynamics (MD) simulation, and compared its partial structure factors and partial pair distribution functions with those of molten $NaNO_2$ and the eutectic mixture of the $NaNO_3$-$NaNO_2$ system showed good additivity for the intermolecular structure because the ionic radius of NO_3 and NO_2 ions are similar owing to the presence of a lone pair on the nitrite ion [6]. After Adya et al. [6], several researchers have reported the MD simulation results of molten alkali nitrates [7-12]. For example, Kato et al. have reported cation dependence of the detailed structural features and ionic dynamics in molten alkali nitrates [11]. They have pointed out that the diffusion constant of small cation is larger than that of large anion. In this study, we have performed MD simulations for molten $NaNO_3$, and obtained new structural information by using several analytical methods.

* Corresponding author: tahara@sci.u-ryukyu.ac.jp

2 Molecular dynamics simulation

The simulation cell contained 1080 ions (Na^+: 216, N^+: 216, and O^-: 648), and NO_3^- was assumed as a rigid ionic molecule in the simulation process. The side length of the simulation cell was 25.3358 Å, which corresponds to the experimental density at the respective temperature of 623 K. The system was annealed at 923 K, and then quenched to 623 K. A time step was set as 5 fs. MD simulation was carried out by using LAMMPS software [13].

The pair potentials used for the simulation were Born-Mayer-Huggins type

$$\phi_{ij} = z_i z_j e^2/r + A_{ij} b \exp[-\varrho(\sigma_i + \sigma_j - r)] \quad (1).$$

The first term on the right-hand side of eq. (1) is Coulomb interaction between ionic charges, where z and e denote valence and unit charges, respectively. The second term denotes repulsion between the ions arising from the overlap of the outer shell of electrons, where A, b, ϱ, and σ denote the Pauling parameter, a constant, a softness parameter, and an ionic radius, respectively. These potential parameters were taken from Adya et al. [6].

3 Results and discussion

3.1 Partial pair distribution functions

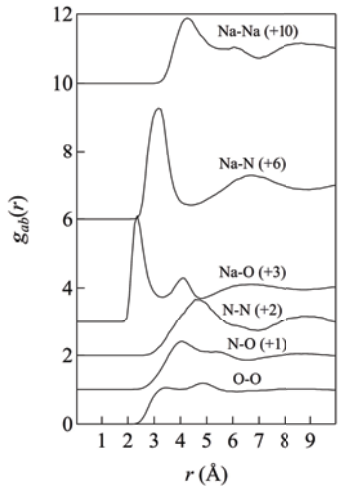

Fig. 1. Partial pair distribution functions $g_{ab}(r)$ for molten $NaNO_3$ at 623 K. The inner molecule interactions for N-O and O-O correlations are not shown for clarity.

Figure 1 shows partial pair distribution functions $g_{ab}(r)$ for molten $NaNO_3$. The $g_{ab}(r)$ values well reproduce earlier simulation results obtained by Adya et al. [6]. We defined the first-coordination length r_c for Na-Na, Na-N, and N-N correlations by using the first-minimum positions in $g_{ab}(r)$, as summarized in Table 1, and these values are used in the analyses described in Sec. 3.3.

Table 1. First-coordination length r_c for Na-Na, Na-N, and N-N correlations.

	Na-Na	Na-N	N-N
r_c [Å]	5.4	4.5	6.7

3.2 Visualization of ionic distribution

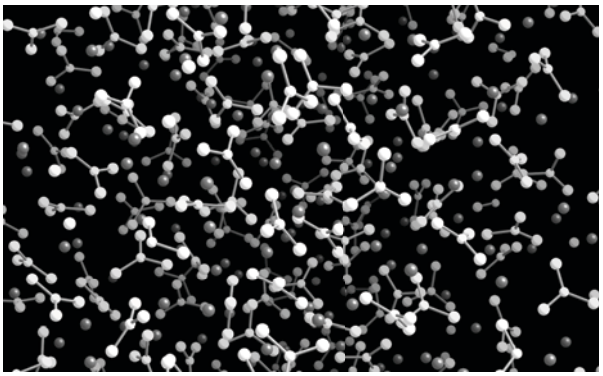

Fig. 2. Snapshot of three-dimensional atomic configurations of molten $NaNO_3$ obtained by MD simulation. Gray spheres denote Na^+ ions. Small and large white spheres denote N and O ions, respectively. N and O ions in a molecule are connected with sticks.

The snapshot of a three-dimensional atomic configuration of molten $NaNO_3$ obtained by MD simulation is visualized in Fig. 2. In this figure, it can be seen that NO_3 molecules are formed by equilateral triangles made of one N^+ and three O^- ions. Na^+ ions are distributed between NO_3^- molecules owing to Coulomb attractions between Na^+ and O^- ions, which is consistent with the relative shorter first-correlation length of Na-N correlation compared to that of Na-Na and N-N correlations, as shown in Fig. 1. Such a structural feature is similar to that of simple molten salts such as NaCl. However, the distributions of Na^+ and NO_3^- ions are slightly asymmetric, because the spectrum patterns of $g_{ab}(r)$ for Na-Na and N-N correlations do not fully correspond with each other. For example, the first peak in g_{NaNa} is narrower than that in $g_{NN}(r)$ and has a shoulder at approximately r = 6 Å, which would be due to the size difference between the Na^+ ion and the NO_3^- ionic molecule.

3.3 Coordination-number and bond-angle distributions

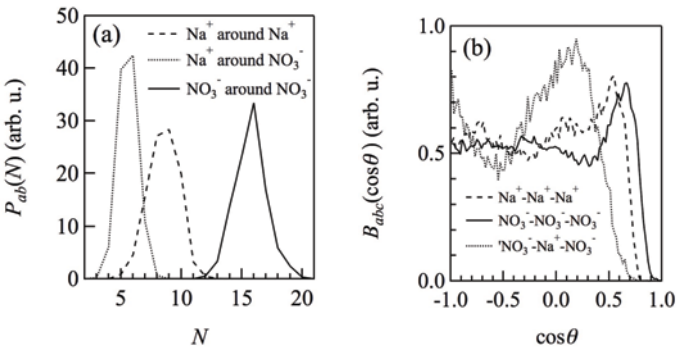

Fig. 2. (a) Coordination-number and (b) bond-angle distributions of Na^+ and NO_3^- ions in molten $NaNO_3$ at 623 K.

The coordination-number distributions $P_{ab}(N)$ (a, b = N^+, NO_3^-) of molten $NaNO_3$ are shown in Fig. 2(a). Since the N^+ ion is located at the center of the NO_3^- molecule, the N^+ ion is regarded as a NO_3^- ionic molecule in this statistics, for example, the coordination number of NO_3^- molecules around a NO_3^- molecule is the same as that of N^+ ions around a N^+ ion. The mean coordination number N_{ab} is summarized in Table 2. The N_{+-} value (= 5.6) for molten $NaNO_3$ is approximately intermediate between that of molten NaCl (N_{+-} = 4.85) and CsCl (N_{+-} = 6.1) [14]. This N_{+-} value is consistent with that reported by Kato et al. (N_{+-} = 5.7), but larger than that for molten $LiNO_3$ (5.0) [11]. The N_{++} value for molten $NaNO_3$ is smaller than the N_{--} value because the first correlation length of Na-Na correlation defined in Sec. 3.1 is shorter than that of N-N correlation. When we consider the shoulder at the high-r side of the first peak in $g_{NaNa}(r)$, the N_{--} and N_{++} are similar to each other. Therefore, the relation between N_{--} and N_{++} largely depends on the definition of the first correlation length of N-N and Na-Na correlations. The N_{--} values of molten NaCl and CsCl are approximately 14 and 17 [14], respectively; therefore, the N_{--} value of molten $NaNO_3$ is also similar to that of simple molten salts.

Fig. 2(b) shows the bond-angle distribution B_{abc} of molten $NaNO_3$. The peaks of B_{+++}, B_{+-}, and B_{---} are found at approximately $\cos\theta = 0.51$ ($\theta = 59°$), 0.17 ($\theta = 80°$), and 0.65 ($\theta = 49°$), respectively, which is also similar to those of simple alkali halides [14]. For molten NaCl and CsCl, the spectral patterns of B_{+++} and B_{---} are almost the same. The difference in the peak positions of B_{+++} and B_{---} for molten $NaNO_3$ reflects the difference in the size of the cation and anion. According to Kato et al. [11], B_{+-+} for molten $NaNO_3$ can be estimated to be 60-90°, which is consistent with our analysis results. Smaller B_{+-+} has been observed for molten $LiNO_3$ [11] due to the smaller size of the Li ion than the Na ion. The B_{+++} and B_{---} values of molten $NaNO_3$ have not been reported as yet.

Table 2. Mean coordination number N_{ab} (ab = ++, +-, --), where + and - denote the Na^+ ion and the NO_3^- ionic molecule, respectively.

	++	+-	--
N_{ab}	8.5	5.6	15.7

3.4 Distribution of Na^+ ions around a NO_3^- ionic molecule

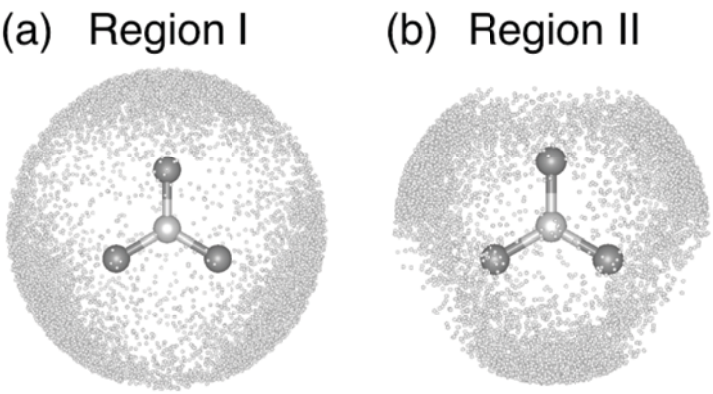

Fig. 3. Statistical distribution of Na^+ ions around a NO_3^- ionic molecule in regions (a) I ($3.1 < r_{NaN} < 3.4$ Å) and (b) II ($2.8 < r_{NaN} < 3.1$ Å) for molten $NaNO_3$ at 623K. The ionic sizes depicted are smaller than the real size for clarity.

The statistical coordinates of Na^+ ions around a NO_3^- molecule within the spherical regions I ($3.1 < r_{NaN} < 3.4$ Å) and II ($2.8 < r_{NaN} < 3.1$ Å) were obtained (Fig. 3); regions I and II

correspond to the top and bottom of the first peak in $g_{NaN}(r)$, respectively. In region I, Na^+ ions are gathered around O^- ions because of the Coulomb attraction. In contrast, the distribution of Na^+ ions in the region II is reverse of that in the region I, because the repulsion of Na-O pairs due to the second term of the right-hand side of eq. (1) becomes larger than the Coulomb attraction. In both of the regions I and II, Na^+ ions are not observed near the N^+ ion due to the repulsion between Na^+ and N^+ ions; the entire right-hand side of eq. (1) shows this repulsion. Such strucutural features are consistent with the analysis results of the cation distribution function around a NO_3^- molecule reported by Kato et al. [11]. The cationic distributions shown in Fig. 3 would help readers in imaging the cation distribution.

3.5 Molecular-orientation correlation

Since NO_3^- is a planar ionic-molecule, the orientation of the molecule can be determined by a normal vector of the plane. The information on the molecular-orientation correlations between NO_3^- molecules is obtained by considering the statistics of dihedral angles θ calculated by the inner product of two normal vectors, where θ is an angle between the normal vectors of NO_3^- molecules. When $\theta = 0$, two molecules are parallel to each other. However, when $\theta = 90°$, the molecules are perpendicular to each other. In this study, two spherical regions III ($4.4 < r_{NN} < 4.6$ Å) and IV ($3.0 < r_{NN} < 3.2$ Å) around the N^+ ion in a central NO_3^- molecule are defined as regions that correspond to the top and bottom of the first peak in $g_{NN}(r)$, respectively. Distance between N^+ ions is regarded as the distance between NO_3^- molecules. The dihedral angle formed by a central molecule and another molecule in the region III (or IV) is calculated as shown in Fig. 4.

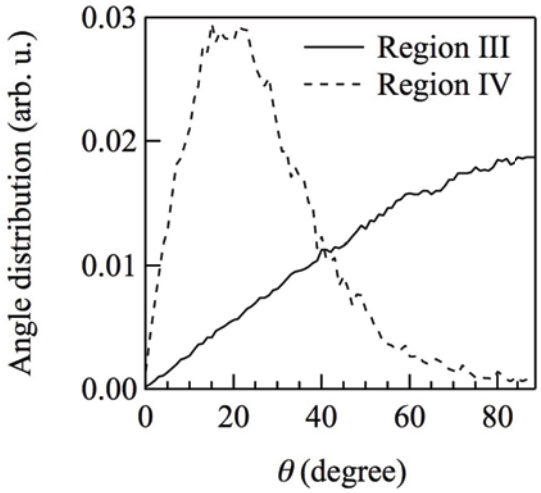

Fig. 4. Distribution of the dihedral angle θ (degree) between NO_3^- ionic molecules.

For the region III, the distribution monotonically increases with increasing θ, and no characteristic peak is observed. In contrast, for the region IV, a characteristic peak is observed at approximately $\theta = 20°$. It is difficult for two NO_3^- ionic molecules to come close to each other within the region III because of their size and shape; however, two NO_3^- molecules can close if the dihedral angle of the molecules becomes small.

4 Summary

The MD simulation for molten $NaNO_3$ was carried out by using the Born-Mayer-Huggins-type potentials. After confirming that the $g_{ab}(r)$ value obtained by the MD simulation well reproduced the results reported in literature, we attempted to obtain the new structural information. We visualized three-dimensional ionic configurations, and showed that Na^+ ions are distributed between NO_3 ions, which is similar to simple molten salts such as NaCl. The coordination-number and bond-angle distributions are similar to those of simple molten salts, except for the variation caused by the different size of the cation and anion. Na^+ ions are basically attracted by O^- ions, and are separated from N^+ ions. When two NO_3^- ions are close to each other, it is need that the dihedral angle of the molecules becomes small.

References

1. C. Y. Zhao, Z. G. Wu, Sol. Energy Mater. Sol. Cells, **95**, 3341 (2011)
2. T. Wang, S. Viswanathan, D. Mantha, R. G. Reddy, Sol. Energy Mater. Sol. Cells, **102**, 201 (2012)
3. D. Mantha, T. Wang, R. G. Reddy, Sol. Energy Mater. Sol. Cells, **118**, 18 (2013)
4. A.G. Fernández, S. Ushak, H. Galleguillos, F. J. Pérez, Sol. Energy Mater. Sol. Cells, **132**, 172 (2015)
5. P. Zhang, X. Xiao, Z. N. Meng, M. Li, Appl. Energy **137**, 758 (2015)
6. A. K. Adya, R. Takagi, K. Kawamura, M. Mikami, J. Mol. Phys. **62**, 227 (1987)
7. T. Kato, K. Machida, M. Oobatake, S. Hayashi, J. Chem. Phys. **89**, 3211 (1988)
8. T. Kato, K. Machida, M. Oobatake, S. Hayashi, J. Chem. Phys. **89**, 7471 (1988)
9. T. Kato, K. Machida, M. Oobatake, S. Hayashi, J. Chem. Phys. **92**, 5506 (1990)
10. T. Kato, K. Machida, M. Oobatake, S. Hayashi, J. Chem. Phys. **93**, 3970 (1990)
11. T. Kato, S. Hayashi, M. Oobatake, K. Machida, J. Chem. Phys. **99**, 3966 (1993)
12. G. Vohringer, J. Richter, Z. Naturforsch. **56 a**, 337 (2001)
13. S. Plimpton, J. Comput. Phys. **117**, 1 (1995)
14. R. L. McGreevy, L. Pusztai, Proc. Royal Soc. **430**, 241 (1990)